Hindawi
Wireless Communications and Mobile Computing
Volume 2022, Article ID 1539056, 10 pages
https://doi.org/10.1155/2022/1539056

Research Article

Pole Extraction of Radar Target in Resonant Region Based on Sliding-Window Matrix Pencil Method

Zhian Deng[1,2], **Tianbao Zhang**[1,2], **Na Li**[3], **Chunjie Zhang**[1,2] and **Weijian Si**[1,2]

[1]*College of Information and Communication Engineering, Harbin Engineering University, Harbin 150001, China*
[2]*Key Laboratory of Advanced Marine Communication and Information Technology, Ministry of Industry and Information Technology, Harbin 150001, China*
[3]*Sichuan Jiuzhou Electric Group Co., Ltd, Mianyang 621000, China*

Correspondence should be addressed to Na Li; 58630950@qq.com

Received 7 December 2021; Accepted 13 April 2022; Published 9 May 2022

Academic Editor: Andrej Hrovat

Copyright © 2022 Zhian Deng et al. This is an open access article distributed under the Creative Commons Attribution License, which permits unrestricted use, distribution, and reproduction in any medium, provided the original work is properly cited.

In the complex battlefield environment, stealth radar target recognition has been paid increasing attentions. Previous studies have demonstrated that the stealth target can be identified well by pole extraction based on matrix pencil method (MPM). However, MPM suffers from the difficulty in setting model order and the time-domain resonant response aliasing problem. This paper proposes a new sliding-window matrix pencil method (SW-MPM) based on dynamic order setting and sliding window. Dynamic order setting scheme is used to overcome the difficulty of setting the order in matrix pencil method, while sliding window can avoid the aliasing problem of time-domain resonant response to some extent. The time-domain scattering data used in SW-MPM are obtained by inverse Fourier transform of the frequency domain scattering data in the resonance region. Taking typical stealth aircraft identification as example, the simulation results verify that the proposed method may extract more number of poles with better azimuth consistency, which is beneficial to improve the accuracy of pole-based target identification.

1. Introduction

In modern electromagnetic spectrum warfare, radar target recognition has attracted more and more attentions [1–4]. Identification of the enemy targets accurately and timely, especially the stealth aircrafts, is the prerequisite for destroying the enemy targets, and any confusion between civilian or friendly targets and enemy targets may cause tragedy [5]. Radar target recognition is closely related to target scattering echoes, and for different targets, the excited characteristics are also different. For typical stealth aircrafts in the optical region, it is difficult to identify them, since radar cross section (RCS) is small according to the target scattering theory [6, 7]. In contrast, for target in the resonance region [8], with the radar signal wavelength close to the target size, RCS is always larger and easy to identify. Moreover, poles extracted from target scattered echoes are very beneficial to target recognition. Poles are mainly related to the size and shape of the target and thus are not sensitive to the target relative attitude and radar polarization [9, 10]. Therefore, poles are considered as robust and effective for the recognition of stealth targets [11].

The first pole extraction algorithm is Prony algorithm [12] presented in 1975. Prony algorithm combined with the singular value decomposition (SVD) can improve the antinoise ability [13]. Prony-based method is sensitive to noise, because it relies on an accurate estimation of the number of target poles, which is difficult to estimate. Matrix pencil method (MPM) [14] is the most widely used method for pole extraction, which has better accuracy, stability, and antinoise performance; compared with Prony method, MPM only needs to construct Hankel matrix with time-domain echo data of the target and then calculate the generalized eigenvalues of the matrices to obtain the target poles. In order to improve the antinoise performance of MPM, Sarkar et al. conducts SVD on the data matrix [15, 16].

The low-rank matrix approximation can suppress the impact of noise and reduce algorithm calculation cost significantly.

In recent years, a lot of research has been devoted to how to apply MPM to pole extraction for radar target [17–19] in real applications. In general, it is difficult to get the actual time-domain echo data, which can be obtained by transforming frequency-domain excited data through simulation. The data transformation from frequency domain to time domain involves the setting of sampling interval, which can be adaptively determined to reduce the computational complexity and time-domain data required [20]. Moreover, in order to get more poles, the wide-band data are required, while in real applications, the data are often narrowband. Thus, Chauveau et al. propose a method [21] based on narrowband data, which avoids extracting target poles using wide-band data. The number of target poles extracted from narrowband data is small, but all of them are main poles with high precision. Some researches make full use of the azimuth consistency of poles to improve the antinoise performance of poles. These methods construct correlation matrices from echo data of multiple directions and then extract target poles by MPM.

Though MPM is one of the most widely used method, it still faces two problems in the pole extraction of complex target [22, 23]. Firstly, the order of the model, namely, the number of target poles, is difficult to determine. The number of poles can be known for simple ideal conductor targets with theoretical solutions, but for complex targets, the number of poles is unknown in advance. An inaccurate estimation of the number of poles may degrade the accuracy of pole extraction greatly. If the number of pole is too small, the real poles of the target will be missed and the extracted poles will have a big deviation from the real poles. If the number of pole is too large, many false poles will be generated and it is impossible to determine which poles are the true ones.

Secondly, it is difficult to distinguish the early time and the late time [24–26] of the target resonant response in time domain. The early time occurs when the wave front of the incident signal interacts with the target and ends when the incident signal completely leaves the target. After the incident signal completely passes through the target, the late time is generated by the gradual decay of the excited current on the target. Due to the propagation delay, there will be an aliasing of early and late time.

In this paper, we propose a new sliding-window matrix pencil method (SW-MPM) based on dynamic order setting and sliding window. Simulations are carried to verify the effectiveness and better azimuth consistency of the proposed method. Our main contributions can be summarized as the following two aspects.

Firstly, we design a sliding window to capture time-domain resonant response for initial pole extraction. The start time of sliding window is estimated based on model of late-time stage and calculation of late-time commencement for various incident wave directions. Then, multiple sets of poles are extracted by sliding through the signal sequence and applying MPM for each sliding window. Among them, the pole whose statistical frequency exceeds a certain threshold is considered as an initial extracted pole. The diversity of different Hankel matrices generated by sliding window can reduce negative effect of time-domain resonant response aliasing, thus improving the reliability and robustness of pole extraction.

Secondly, we obtain the final stable poles by dynamic order setting on initial extracted pole sets. Relevant studies show that the true poles will converge with the variation of order, while false poles are irregularly distributed in the complex plane. Therefore, we traverse model order and generate another set of poles on the basis of initial pole extraction. Histogram statistics of poles extracted from diverse orders are carried out, and any pole whose related occurrence frequency exceeds another threshold is considered as a true pole.

2. Target Time-Domain Resonant Response Acquisition

The radar target time-domain resonant response can be considered as an output of a linear time-invariant radar system. In actual radar system, we use a narrow pulse signal to illuminate the target, and the scattering response signal at this time is the time-domain resonant response. However, it is difficult to get the actual measurement data of military targets, especially for stealth aircraft. In this paper, a professional electromagnetic simulation software, is used to generate the frequency-domain scattering data based on geometry model of radar target. Then, the time-domain resonant response is obtained through time-frequency data transformation. Target time-domain resonant response can be subdivided into early time and late time. The singularity expansion method (SEM) proves that the late time contains the target pole information. This section first briefly introduces singularity expansion theory and then describes the process of the time-frequency data transformation. Finally, a physical model describing early-time and late-time stages of a simple target is given.

2.1. Singularity Expansion Theory. Singularity expansion theory is an important theory when the late-time stage of radar echo is studied. The theory systematically describes the echo characteristics, transfer function, and properties of radar targets in the resonance region. Time response of the radar target in the resonance region can be expressed as the sum of attenuation exponents on the complex plane [27, 28],

$$y(t) = \sum_{i=1}^{M} R_i e^{s_i t}, \tag{1}$$

where M is the number of poles, R_i is the residue, and $s_i = \sigma_i + j\omega_i$ is the pole. σ_i and ω_i represent the attenuation factor and the attenuation frequency, respectively.

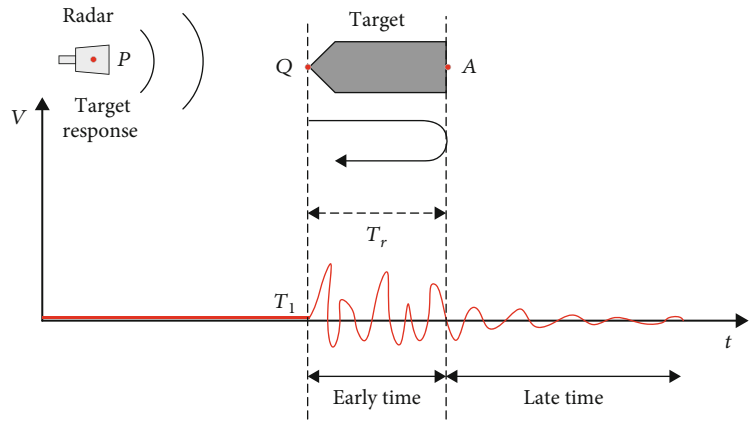

Figure 1: Early- and late-time boundaries.

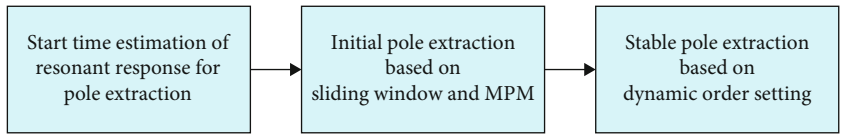

Figure 2: Overview of the proposed sliding-window matrix pencil method.

In Laplace-domain, the transfer function of radar target scattering can be expressed as the sum of a rational function and an integral function.

$$H(s) = \sum_{i=1}^{M} \frac{R_i}{s - s_i} + C(s). \tag{2}$$

The integral part $C(s)$ corresponds to the early-time stage of the system in time domain, which describes the scattering characteristics of the radar target. The rational part corresponds to the late-time stage, which describes the pole characteristics of the radar target.

2.2. Frequency-Domain Data. The frequency-domain response of the radar target can be obtained either by simulation calculation or actual measurement. It is usually difficult to obtain actual measurement data for complex military targets, so electromagnetic simulation software, such as FEKO, is generally used to calculate scattering data by moment method [29–31].

The scattering data in the frequency-domain can be expressed as

$$\widehat{E}_s(\omega) = H(\omega), 0 < \omega < \omega_c, \tag{3}$$

where ω_c is the maximum frequency and $H(\omega)$ is the impulse response of the target in the frequency domain. If the time-domain incident signal can be expressed as a Sinc function

$$e_i(t) = Sa(\omega_c t), \tag{4}$$

the frequency-domain expression of scattering echo is

$$E_s(\omega) = E_i(\omega) \cdot H(\omega) = \begin{cases} \dfrac{\pi}{\omega_c} H(\omega) & |\omega| \le \omega_c, \\ 0 & |\omega| > \omega_c. \end{cases} \tag{5}$$

We consider that the time-domain impulse response in the fact is a real signal, and $H(\omega)$ with conjugate symmetry can be expressed as

$$E_s(\omega) = \begin{cases} \dfrac{\pi}{\omega_c} \cdot \widehat{E}_s(\omega) & 0 \le \omega \le \omega_c, \\ \dfrac{\pi}{\omega_c} \cdot \widehat{E}_s^*(-\omega) & -\omega_c < \omega \le 0. \end{cases} \tag{6}$$

Thus, the time-domain scattering echo signal is

$$e_s(t) = e_i(t) * h(t) = \frac{2\pi}{\omega_c} \cdot \mathrm{Re}\{\widehat{e}_s(t)\}, \tag{7}$$

$$\widehat{e}_s(t) = \frac{1}{2\pi} \int_0^{\omega_c} \widehat{E}_s(\omega) e^{jwt} d\omega. \tag{8}$$

The above derivation shows that time-domain resonant response is obtained directly through the inverse Fourier transform of frequency-domain truncated data. That is to say, when the incident signal of the target is a Sinc pulse, the reflected echo is time-domain resonant response. In order to suppress time-domain data energy leakage caused by data truncation in the frequency domain, we smooth the time-domain resonant response by hamming window.

2.3. Early-Time and Late-Time Stage. The interaction between incident signal and target is shown in Figure 1.

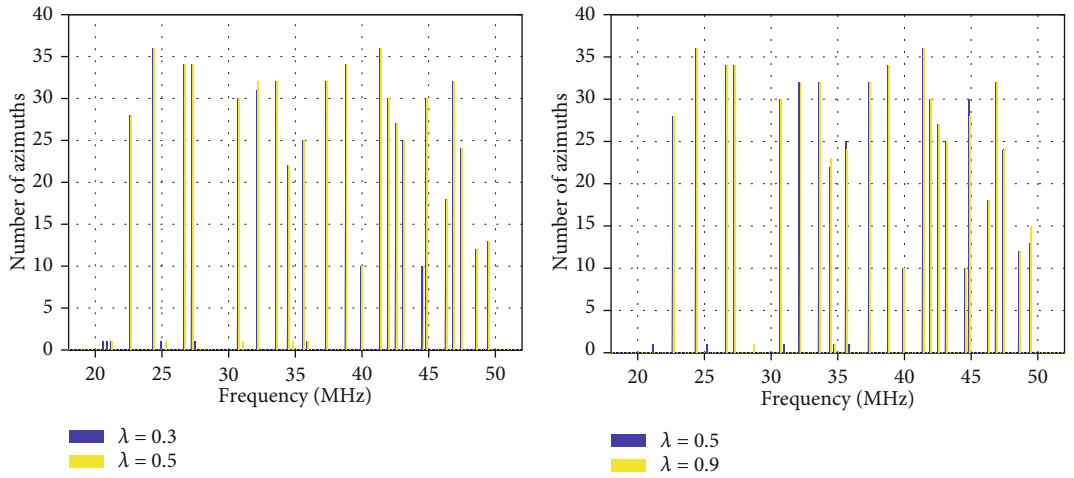

(a) $\lambda = 0.3, 0.5$ (b) $\lambda = 0.5, 0.9$

Figure 3: Number of azimuths for pole frequency with different sliding window probability thresholds.

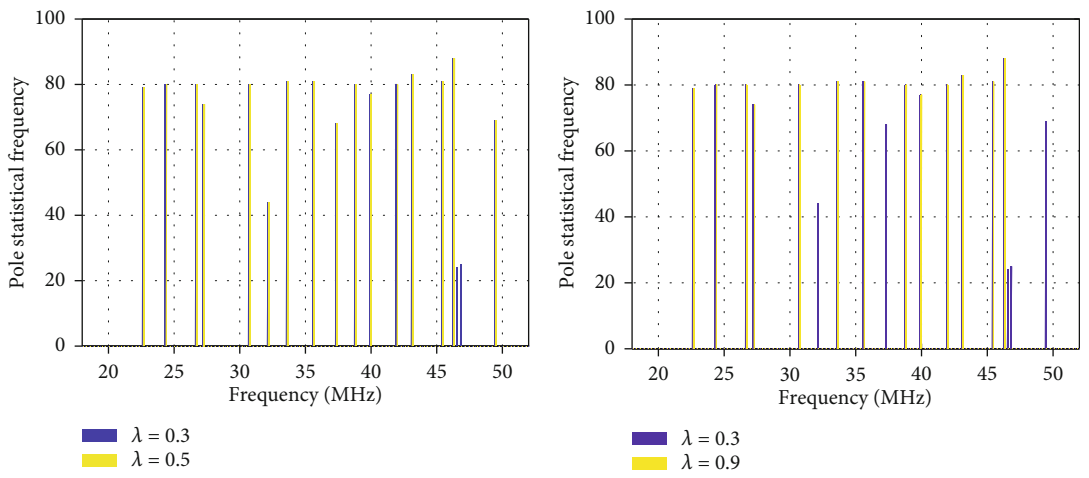

(a) $\lambda = 0.3, 0.5$ (b) $\lambda = 0.3, 0.9$

Figure 4: Comparison of pole statistical frequency in single azimuth for different sliding window probability thresholds.

Assuming that the signal radiates from the position P, the receiving position is also P. The incident wave reaches the target at time T_1, and the early-time stage begins at this time. The late-time stage start time is often defined as

$$t_1 = T_1 + 2T_r + T_e. \tag{9}$$

T_e is the pulse width of the incident signal. Due to the propagation delay, the response generated at position Q and the response generated at position A have a time difference of T_r. The advantage of this definition is that the late-time stage is not aliased with the early-time stage, but the late-time sequence is incomplete which causes the loss of pole information. More importantly, for complex radar target, the start time of late-time stage always changes with the incident direction and difficult to estimate for noncooperative target.

The late-time stage has already occurred at position Q; thus, we consider the late-time stage starts at

$$t_2 = T_1 + T_r + T_e. \tag{10}$$

This definition of the late-time stage can contain all information about poles, but there are also drawbacks. Obviously, one major drawback is that time delay causes an aliasing of early-time and late-time stage. The aliasing is difficult to eliminate, which may lead to pole loss and pole extraction errors. In addition, the variation of the incident signal direction may also render different start times of the late-time stage. To overcome these drawbacks, sliding window is adopted to capture the echo data used for pole extraction. Through the diversity effect of sliding window on the start of late-time stage, the aliasing data between late-time and early-time stage are preserved and explored, while interference from early-time data is reduced to some extent.

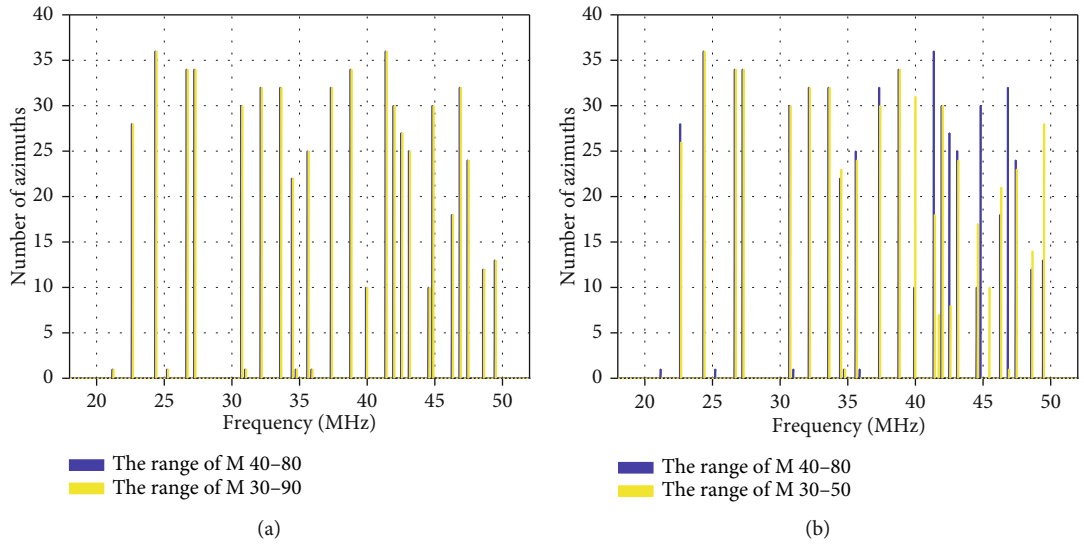

Figure 5: Number of azimuths for pole frequency with different model order ranges.

The typical stealth target studied in this paper belongs to the complex target. Combining with the above discussions, the method for obtaining the start time for pole extraction is given as follows. Firstly, we obtain the time-domain resonant response for each discrete azimuth, which is evenly distributed and spaced by 10 degrees. Secondly, t_2 is calculated based on the geometric relationship between aircraft and incident electromagnetic wave from different azimuth. Finally, the smallest t_2 is selected as the start time for pole extraction.

3. Proposed Sliding-Window Matrix Pencil Method

An overview of the proposed SW-MPM method based on sliding window and dynamic order setting is shown in Figure 2. Firstly, start time of resonant response for pole extraction is obtained based on the method proposed in the last paragraph of Section 3.2. Then, a sliding window is used to generate the signal sequence, and a set of poles is obtained based on the signal sequence in the window using MPM. The window with a fixed width slides through the signal sequence, and multiple sets of poles can be obtained upon different start sliding times. For each fixed model order, we can calculate the statistical histogram to extract a corresponding initial set of poles, whose statistical frequency exceed a certain threshold. Finally, we traverse model order and generate another set of poles on the basis of initial pole extraction for each fixed model order. The final stable poles are calculated by choosing the set of poles, whose statistical frequency exceed another certain threshold.

3.1. Initial Pole Extraction Based on Sliding Window and MPM. To overcome aliasing of early-time stage and late-time stage and improve the azimuth consistency of poles, we deploy the sliding window to capture required time-domain data for initial pole extraction. The diversity of sliding window can improve the reliability and robustness of

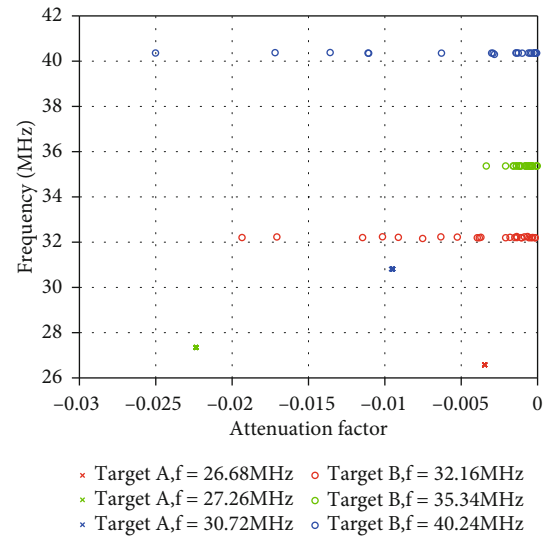

Figure 6: Pole aggregation phenomenon under different model orders.

pole extraction. Firstly, the sliding window is used to generate signal sequence and construct the related Hankel matrix. Then, we establish the matrix pencil based on the special relationship between the eigenvalues of the Hankel matrix and extract initial poles by solving the generalized eigenvalues of the matrix.

Denote the whole signal sequence as $y(t)$, and the related discrete form is

$$y(n) = \sum_{i=1}^{M} R_i z_i^n, \quad n = 1, 2, \cdots N. \tag{11}$$

A set of poles is extracted through a sliding window for the signal sequence $y(n)$ with a total length of N. Each sliding window corresponds to a Hankel matrix, and a total

Table 1: Pole frequency comparison of target A.

Pole frequency of SW-MPM (MHz)	4.76; 7.64; 14.57; 18.03; 24.38; 26.68; 27.26; 30.72; 32.16; 33.61; 37.36; 38.80; 41.39
Pole frequency of MPM (MHz)	14.57; 18.03; 24.38; 33.61; 38.80; 41.39

Table 2: Pole frequency comparison of target B.

Pole frequency of SW-MPM (MHz)	32.16; 35.34; 40.24; 52.64; 65.63; 67.36; 69.38; 71.68; 78.89
Pole frequency of MPM (MHz)	32.16; 35.34; 52.64; 67.36; 69.38; 71.68; 78.89

number N_c sliding window is applied. The window slid from the beginning of the sequence $n = 1$ to the moment $n = N_c$. Define the Hankel matric $Y^{(i)}$ with the ith sliding window:

$$Y^{(i)} = \begin{bmatrix} y_i(1) & y_i(2) & \cdots & y_i(L) \\ y_i(2) & y_i(3) & \cdots & y_i(L+1) \\ \vdots & \vdots & \ddots & \vdots \\ y_i(N-L-1) & y_i(N-L) & \cdots & y_i(N) \end{bmatrix}. \tag{12}$$

y_i represents a sample of the used signal sequence, and L is the pencil parameter.

In order to reduce noise contained in the received echo signal, we deploy SVD to remove the small nonzero singular value and reconstruct Hankel matrix,

$$Y^{(i)} = \begin{bmatrix} U\, U' \end{bmatrix} \begin{bmatrix} \Sigma & 0 \\ 0 & \Sigma' \end{bmatrix} \begin{bmatrix} V^H \\ V'H \end{bmatrix}, \tag{13}$$

where $\Sigma = \text{diag}\{\sigma_1, \sigma_2, \cdots, \sigma_M\}$ contains the corresponding larger eigenvalues of the pole information. $\sigma_1, \sigma_2, \cdots, \sigma_M$ is the maximum M singular values of $Y^{(i)}$. Σ' is a diagonal matrix containing small eigenvalues of noise information. $\tilde{Y}^{(i)} = U\Sigma V^H$ is the low rank approximation of $Y^{(i)}$. We can get $\tilde{Y}_1^{(i)}$ with the last column of $Y^{(i)}$ deleted and $\tilde{Y}_2^{(i)}$ with the first column deleted,

$$\tilde{Y}^{(i)} = \begin{bmatrix} \tilde{Y}_1{}^{(i)} & y_0 \end{bmatrix} = \begin{bmatrix} y_L & \tilde{Y}_2{}^{(i)} \end{bmatrix}, \tag{14}$$

where $\tilde{Y}_1^{(i)} = U\Sigma V_1^H$ and $\tilde{Y}_2^{(i)} = U\Sigma V_2^H$. Target pole z_i is the generalized eigenvalue of the matrix with respect to $\{\tilde{Y}_1{}^{(i)}, \tilde{Y}_2{}^{(i)}\}$. As a result, target pole z_i can be obtained by solving the eigenvalue of $\tilde{Y}_1^{(i)+}\tilde{Y}_2^{(i)}$, where $\tilde{Y}_1^{(i)+}$ is the generalized inverse of $\tilde{Y}_1^{(i)}$.

For each sliding window, we can obtain M poles according to the above description. Walk through all the sliding windows to get a set of poles containing $N_c * M$ poles. Then, histogram statistics are carried out on the pole frequency of the pole set obtained by the sliding window. The statistical histogram is divided into multiple regions according to the extracted highest pole frequency $F_{\max}$. Each region has a length of len, indicating the allowable fluctuation range of the pole frequency. If the statistical frequency of a pole falling within a certain interval N_{pole} exceeds the threshold value λ, then the median value of all the poles in the interval is considered as an initial extracted pole frequency.

3.2. Stable Pole Extraction Based on Dynamic Order Setting. The selection of pole number (model order) M has a great influence on the pole extraction accuracy. For simple ideal conductor targets, the number of poles can be calculated according to related theory. For complex radar target, such as typical stealth aircrafts, the number of poles is unknown and difficult to estimate.

One of the most widely used methods for determining M is

$$\min_M \sum_{k=1}^{N} (y_{rec}(k) - y_{cal}(k))^2. \tag{15}$$

Among them, $y_{\text{rec}}(k)$ is the time-domain signal of pole reconstruction, $y_{\text{cal}}(k)$ is the actual signal, and N is the sampling points of target echo signal used for pole extraction. Due to noise interference, it is difficult to choose an appropriate pole number for this method. Moreover, for any fixed pole number, it may render false poles caused by response aliasing between early-time and late-time stage for real applications.

In the proposed SW-MPM, instead of using a fixed M, a dynamic range of M is given to overcome the order ambiguity [32, 33]. Our research results show that the real target poles will converge with the variation of M. The real poles obtained by each simulation are densely distributed, while the false poles are scattered irregularly in the complex plane. Through the statistics of poles extracted from different M, the real poles can be determined and false poles are removed. Related steps are given as follows:

(1) Set the dynamic range of order $M_{\min}$~$M_{\max}$. The value of the minimum $M_{\min}$ is at least 10, and the value of the maximum $M_{\max}$ is generally less than $N/6$

(2) For each fixed M, a set of initially stable poles is obtained as described in Section 3.1

(3) Histogram statistics of poles for all dynamic orders are carried out. Histogram intervals are divided according to the highest frequency $F_{\max}$ extracted

at $M = M_{\max}$. Each interval has a length of len, and there are $F_{\max}$/len intervals in total. $N_p(i)$ represents the number of poles falling in the i interval

(4) If $N_p(i)$ exceeds a certain threshold value ζ, then the median of all pole frequencies in the interval $N_p(i)$ is considered as one ultimate stable pole frequency. Otherwise, all poles in this region are considered as false poles and discarded. The threshold value ζ is generally set as the smallest integer exceeds $0.8 * (M_{\max} - M_{\min} + 1)$

4. Simulation Results and Analysis

In this section, the time-domain echo data are obtained by inverse fast Fourier transform of frequency-domain RCS data, which are generated by FEKO simulation software on two typical stealth aircrafts, called A and B. We firstly discuss the effect of the sliding window probability threshold on pole extraction. Next, we study the effect of dynamic order setting on pole extraction. Then, we compare the pole extraction performance of MPM and the proposed SW-MPM. Finally, we compare the azimuth consistency of poles extracted by MPM and SW-MPM. For two typical stealth aircrafts, we test the pole extraction performance for 36 discrete azimuths, which are evenly distributed within the 360 degrees and spaced by 10 degrees.

4.1. Effect of Sliding Window Probability Threshold on Pole Extraction. Due to the variation of radar target shape and feature size, the late-time stage for different radar targets is different. Even for the same complex target, the late-time stage varies with the different incident wave directions (azimuths). The efficient acquisition of late-time stage data has great influence on pole extraction. If the start of late-time stage is too early, the early-time signal will be introduced, which will generate false poles. If the start of late-time stage is too late, the precision and antinoise performance of pole extraction will degrade due to the rapid attenuation of signal energy. Thus, sliding windows are introduced to explore adversity of different start times of late-time stage data and eliminate the negative effect of late-time stage and early-time stage aliasing problem.

Figures 3 and 4 show the effect of sliding window probability threshold on pole extraction. Figure 3 focuses on the influence of sliding window probability threshold on the azimuth of pole occurrence, while Figure 4 shows the relationship between pole statistical frequency and sliding window probability threshold when the azimuth is constant. Sliding window probability threshold λ is set to select alternate poles. That is, with the movement of the whole N_c sliding window, the poles extracted appearing more than $\lambda * N_c$ are considered as the alternative poles. As can be seen from Figure 3, when λ is selected as 0.3 and 0.5, the extraction of main poles is basically the same; when λ is selected as 0.9, the extraction of individual poles will be slightly worse. As can be seen from Figure 4, the smaller λ is, the more poles meet the conditions. Too large λ will lead to the missing of some real poles. If λ is too small, some interference and false

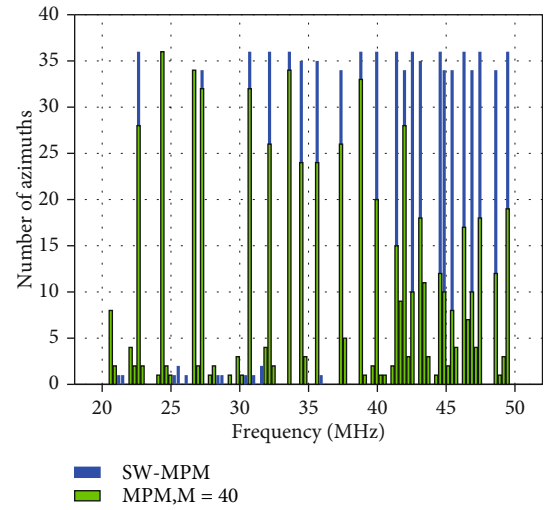

Figure 7: Comparison of pole extraction between MPM and SW-MPM for target A.

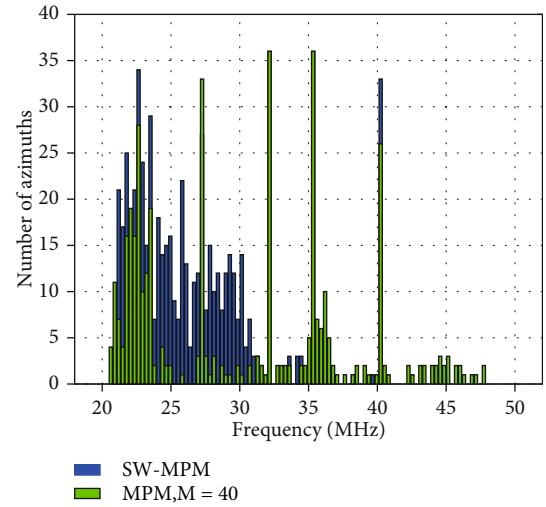

Figure 8: Comparison of pole extraction between MPM and SW-MPM for target B.

poles are extracted and the computational complexity of the system increases. Therefore, it is suitable to choose the probability threshold between 0.5 and 0.8.

4.2. Effect of Dynamic Order Setting on Pole Extraction. Figure 5 shows the effect of dynamic order setting on pole extraction. The horizontal axis represents the pole frequency, and the vertical axis represents the number of azimuths when the related poles appear. Taking coordinate (24.38 MHz, 36) for example, it means that the frequency of 24.38 MHz can be extracted in 36 evenly divided azimuths. As seen in Figure 5(a), when the range of model order is set to 30 : 90, the extraction result is similar to that of 40 : 80, but the former range renders higher computational complexity. As seen in Figure 5(b), when the range is set to 30 : 50, the pole extraction result between 40 MHz and 50 MHz is obviously inferior to 40 : 80. For example,

the frequency of 41.39 MHz can be extracted from all 36 azimuths when the range is set to 40 : 80, while 41.39 MHz can only be extracted from less than 20 azimuths in range 30 : 50. If the model order range is set too large, unnecessary interference and higher computational complexity may be introduced. If the range is set too small, the diversity characteristics of model order are not fully utilized, leading to the loss of real poles. Therefore, it can be seen that pole extraction performance is robust to the dynamic order setting range, and the range of 40 : 80 is reasonable in our simulations.

Figure 6 shows the pole aggregation phenomenon of some poles extracted, which will provide a theoretical basis for dynamic order setting. The figure shows the two-dimensional distribution of some poles, where the horizontal axis represents the attenuation factor and the vertical axis represents the pole frequency. The model order varies from 40 to 80, and each pole frequency can occur up to 41 times with the variation of model order. For pole with frequency 27.26 MHz of target A, 38 similar poles are counted in the simulations. And for pole with frequency 35.34 MHz of target B, 35 similar poles can also be counted even if the attenuation factor is slightly different. Thus, it is reasonable to use the diversity of model order to improve the performance of pole extraction because of the aggregation of poles under different model orders.

4.3. Comparison of MPM and the Proposed SW-MPM. In this section, we compare the pole extraction results of MPM and SW-MPM. Tables 1 and 2 show the pole extraction results of targets A and B. It is shown that the number of poles extracted by SW-MPM is significantly more than that by MPM. SW-MPM can extract 13 pole frequencies for target A and 9 pole frequencies of target B. In contrast, MPM can only extract 6 pole frequencies of A and 7 pole frequencies of B. Furthermore, the poles extracted by the SW-MPM method contain all poles extracted by the MPM method.

Figures 7 and 8 compare pole extraction of target A and target B, respectively, by MPM and SW-MPM. As can be seen from these figures, for common poles, poles extracted by SW-MPM appear in more azimuths, which indicates that these poles have better robustness and antinoise performance. As can be seen from Figures 7 and 8, SW-MPM performs better than MPM in pole extraction for the same target. The main reason is that MPM suffers from the difficulty of setting the model order and the influence of early-time stage and late-time stage aliasing. In contrast, the proposed SW-MPM avoids these problems by dynamic order setting and sliding window, which both can explore diversity advantages.

4.4. Analysis of Azimuth Consistency. For 36 azimuths in our simulations, we calculate the statistical frequency of poles occurring in each azimuth. If a certain pole frequency appears in more azimuths, we consider that the pole has higher reliability and better azimuth consistency, which is better for radar target recognition. We express the degree of azimuth consistency of poles by the so-called probability

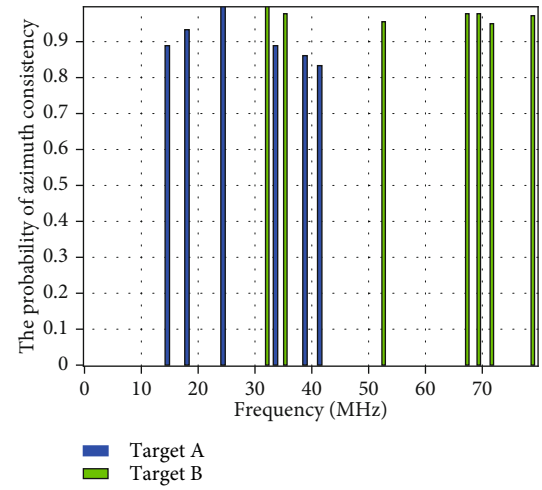

Figure 9: The probability of pole azimuth consistency distribution of MPM.

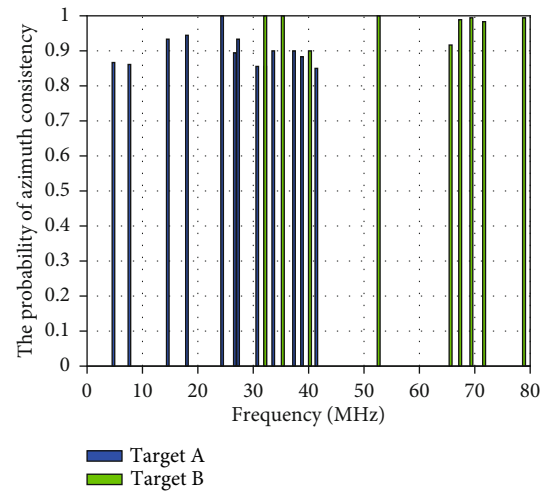

Figure 10: The probability of pole azimuth consistency distribution of SW-MPM.

of azimuth consistency. The probability is defined as the ratio of the number of azimuths that the pole appears to the total number of discrete azimuths.

Figures 9 and 10 show the azimuth consistency probability of the pole extracted in Section 4.3. It can be seen that for the same pole, the azimuth consistency extracted by SW-MPM is better than the MPM. For pole frequency 14.57 MHz of target A, the azimuth consistency probability of SW-MPM and MPM is 94.28% and 89.02%, respectively; for another pole frequency 33.61 MHz, the azimuth consistency probability of the two methods is 90% and 88.58%, respectively. For pole frequency 52.64 MHz of target B, the azimuth consistency probability of the two methods is 100% and 96.98%, respectively. For another pole frequency of 71.68 MHz, the probabilities of two methods are 97.14% and 95.88%, respectively. Therefore, the azimuth consistency of the poles extracted by the proposed SW-MPM is significantly better than that of MPM.

5. Conclusions

We proposed SW-MPM based on sliding window and dynamic order setting for pole extraction. Compared with traditional MPM method, SW-MPM can avoid the aliasing problem of time-domain resonant response to some extent and extracts more reliable poles by exploring diversity advantages of sliding window and dynamic order setting.

Our simulations on two typical stealth aircrafts verify the effectiveness and improvement of the proposed SW-MPM in pole extraction. SW-MPM can extract more poles than the MPM method for the same target. Moreover, for common poles, the azimuth consistency of poles obtained by SW-MPM is better than that of MPM. In our future work, we will test the performance of the proposed SW-MPM in more complicated battlefield electromagnetic environment, including more kinds of complex radar target and noise interference.

Data Availability

The data used to support the findings of this study are available from the corresponding author upon request.

Conflicts of Interest

The authors declare that there are no conflicts of interest regarding the publication of this paper.

Acknowledgments

This work was financially supported by the National Natural Science Foundation of China (Grant No. 61971155 and 61801143), Natural Science Foundation of Heilongjiang Province of China (Grant No. JJ2019LH1760), the Fundamental Research Funds for the Central Universities (Grant No. 3072020CF0814), Aeronautical Science Foundation of China (Grant No. 2019010P6001), and Heilongjiang Postdoctoral Foundation (Grant No. LBH-Z2009).

References

[1] Y. X. Sun, H. Q. Xiong, D. K. P. Tan, T. X. Han, and R. Du, "Moving target localization and activity/gesture recognition for indoor radio frequency sensing applications," *IEEE Sensors Journal*, vol. 21, no. 21, pp. 24318–24326, 2021.

[2] D. B. Zhao and H. Li, "Radar target recognition based on central moment feature and GA-BP neural network," *Infrared and Laser Engineering*, vol. 47, no. 8, article 0826005, 2018.

[3] K. Wu, J. Xiao, Y. Yi, M. Gao, and L. M. Ni, "FILA: fine-grained indoor localization," in *2012 Proceedings IEEE INFOCOM*, pp. 2210–2218, Orlando, FL, USA, March 2012.

[4] M. Zhou, Y. X. Lin, N. Zhao, Q. Jiang, X. L. Yang, and Z. S. Tian, "Indoor WLAN intelligent target intrusion sensing using ray-aided generative adversarial network," *IEEE Transactions on Emerging Topics in Computational Intelligence*, vol. 4, no. 1, pp. 61–73, 2020.

[5] B. Borden, "Radar scattering centre localization by subspace fitting," *Inverse Problems*, vol. 17, no. 5, pp. 1483–1491, 2001.

[6] X. W. Liu, J. Z. Li, Y. Zhu, and S. J. Zhang, "Scattering characteristic extraction and recovery for multiple targets based on time frequency analysis," *Applied Computational Electromagnetics Society Journal*, vol. 35, no. 8, pp. 962–970, 2020.

[7] H. Jia, X. Li, and X. Meng, "Rigid and elastic acoustic scattering signal separation for underwater target," *Journal of the Acoustical Society of America*, vol. 142, no. 2, pp. 653–665, 2017.

[8] O. Lalakulich, E. A. Paschos, and G. Piranishvili, "Resonance production by neutrinos: The second resonance region," *Physical Review D*, vol. 74, no. 1, article 014009, 2006.

[9] D. L. Moffatt, "Transient response characteristics in identification and imaging," *IEEE Transactions on Antennas and Propagation*, vol. 29, no. 2, pp. 192–205, 1981.

[10] Y. Gong, S. Q. Xiao, and B. Z. Wang, "Synthesis of sparse planar arrays with multiple patterns by the generalized matrix enhancement and matrix pencil," *IEEE Transactions on Antennas and Propagation*, vol. 69, no. 2, pp. 869–881, 2021.

[11] A. Ponsford, L. Sevgi, and H. C. Chan, "An integrated maritime surveillance system based on high-frequency surface-wave radars. 2. Operational status and system performance," *IEEE Antennas and Propagation Magazine*, vol. 43, no. 5, pp. 52–63, 2001.

[12] M. L. Blaricum and R. Mittra, "A technique for extracting the poles and residues of a system directly from its transient response," *IEEE Transactions on Antennas and Propagation*, vol. 23, no. 6, pp. 777–781, 1975.

[13] D. W. Tufts and R. Kumaresan, "Estimation of frequencies of multiple sinusoids: making linear prediction perform like maximum likelihood," *Proceedings Of IEEE*, vol. 70, no. 9, pp. 975–989, 1982.

[14] Y. B. Hua and T. K. Sarkar, "Generalized pencil-of-function method for extracting poles of an EM system from its transient response," *IEEE Transactions on Antennas and Propagation*, vol. 37, no. 2, pp. 229–234, 1989.

[15] T. K. Sarkar and O. Pereira, "Using the matrix pencil method to estimate the parameters of a sum of complex exponentials," *IEEE Antennas and Propagation Magazine*, vol. 37, no. 1, pp. 48–55, 1995.

[16] T. K. Sarkar, S. Park, and J. Koh, "Application of the matrix pencil method for estimating the SEM (singularity expansion method) poles of source-free transient responses from multiple look directions," *IEEE Transactions on Antennas and Propagation*, vol. 48, no. 4, pp. 612–618, 2000.

[17] L. Bernard, S. Goondram, B. Bahrani, A. A. Pantelous, and R. Razzaghi, "Harmonic and interharmonic phasor estimation using matrix pencil method for phasor measurement units," *IEEE Sensors Journal*, vol. 21, no. 2, pp. 945–954, 2021.

[18] M. Bhuiyan, E. V. Malyarenko, M. A. Pantea, D. Capaldi, A. E. Baylor, and R. G. Maev, "Time-0," *Journal of Electrical and Computer Engineering*, vol. 2015, 10 pages, 2015.

[19] Y. Terriche, S. Golestan, J. M. Guerrero, D. Kerdoune, and J. C. Vasquez, "Matrix pencil method-based reference current generation for shunt active power filters," *IET Power Electronics*, vol. 11, no. 4, pp. 772–780, 2018.

[20] I. S. Choi, H. Lee, and H. T. Kim, "Natural frequency extraction using late-time evolutionary programming-based CLEAN," *IEEE Transactions on Antennas and Propagation*, vol. 51, no. 12, pp. 3285–3292, 2003.

[21] J. Chauveau, N. D. Beaucoudrey, and J. Saillard, "Determination of resonance poles of radar targets in narrow frequency

bands," in *2007 European Radar Conference*, pp. 122–125, Munich, Germany, Oct 2007.

[22] L. Man, X. Wei, C. Dong, and Z. Xiao, "Poles extracting and analyzing of complex stealth target based on matrix pencil method," in *2014 IEEE International Conference on Computer and Information Technology*, pp. 894–898, Xi'an, China, September 2014.

[23] H. Hu and K. L. Wu, "A generalized coupling matrix extraction technique for bandpass filters with uneven-Qs," *IEEE Transactions on Microwave Theory and Techniques*, vol. 62, no. 2, pp. 244–251, 2014.

[24] O. H. Chad, L. C. Vaughan, and L. Hoi-Shun, "Late-time estimation for resonance-based radar target identification," *IEEE Transactions on Antennas and Propagation*, vol. 62, no. 11, pp. 5865–5871, 2014.

[25] C. Hargrave, A. Abbosh, V. Clarkson, and N. Shuley, "Radar target identification: estimating the start of the late time resonant response," in *2013 International Conference on Radar*, pp. 335–340, Adelaide, SA, Australia, Sept 2013.

[26] L. Carin, H. Yu, Y. Dalichaouch, and A. R. Perry, "On the wideband EMI response of a rotationally symmetric permeable and conducting target," *IEEE Transactions on Geoscience and Remote Sensing*, vol. 39, no. 6, pp. 1206–1213, 2001.

[27] A. M. Alzahed, S. Mikki, and Y. Antar, "Electromagnetic machine learning for inverse modeling using the spatial singularity expansion method," *IEEE Journal on Multiscale and Multiphysics Computational Techniques*, vol. 5, pp. 59–71, 2020.

[28] S. Licul and W. A. Davis, "Unified frequency and time-domain antenna modeling and characterization," *IEEE Transactions on Antennas and Propagation*, vol. 53, no. 9, pp. 2882–2888, 2005.

[29] S. Clarke and U. Jakobus, "Dielectric material modeling in the MoM-based code FEKO," *IEEE Antennas and Propagation Magazine*, vol. 47, no. 5, pp. 140–147, 2005.

[30] S. R. Chai, L. X. Guo, K. Li, and L. Li, "Combining CS with FEKO for fast target characteristic acquisition," *IEEE Transactions on Antennas and Propagation*, vol. 66, no. 5, pp. 2494–2504, 2018.

[31] J. P. Sijabat and T. Indriyanto, "Radar Cross section analysis of unmanned combat aerial vehicle (UCAV) using FEKO software," *AVIA*, vol. 2, no. 2, 2021.

[32] W. B. Deng, *Poles extraction and characteristic analysis of radar target in resonant region*, Harbin Institute of Technology, Harbin, China, 2012.

[33] C. Malzer and M. Baum, "Constraint-based hierarchical cluster selection in automotive radar data," *Sensors*, vol. 21, no. 10, article 3410, 2021.